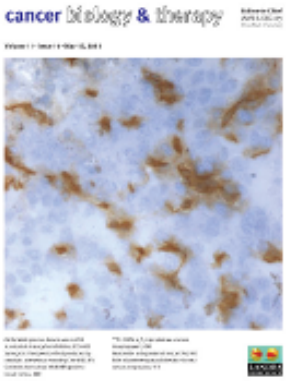

Cancer Biology & Therapy
Publication details, including instructions for authors and subscription information:
http://www.tandfonline.com/loi/kcbt20

Conjugated PDT drug: Photosensitizing activity and tissue distribution of PEGylated pheophorbide a

Valentina Rapozzi, Marina Zacchigna, Stefania Biffi, Chiara Garrovo, Francesca Cateni, Marco Stebel, Sonia Zorzet, Gian Maria Bonora, Sara Drioli & Luigi Xodo

Published online: 01 Sep 2010.

To cite this article: Valentina Rapozzi, Marina Zacchigna, Stefania Biffi, Chiara Garrovo, Francesca Cateni, Marco Stebel, Sonia Zorzet, Gian Maria Bonora, Sara Drioli & Luigi Xodo (2010) Conjugated PDT drug: Photosensitizing activity and tissue distribution of PEGylated pheophorbide a, Cancer Biology & Therapy, 10:5, 471-482, DOI: 10.4161/cbt.10.5.12536

To link to this article: http://dx.doi.org/10.4161/cbt.10.5.12536

RESEARCH PAPER

Cancer Biology & Therapy 10:5, 471-482; September 1, 2010; © 2010 Landes Bioscience

Conjugated PDT drug

Photosensitizing activity and tissue distribution of PEGylated pheophorbide *a*

Valentina Rapozzi,[1,†] Marina Zacchigna,[2,†] Stefania Biffi,[5] Chiara Garrovo,[5] Francesca Cateni,[2] Marco Stebel,[4] Sonia Zorzet,[4] Gian Maria Bonora,[3] Sara Drioli[3] and Luigi E. Xodo[1,*]

[1]Department of Biomedical Science and Technology; School of Medicine; University of Udine; Udine, Italy; [2]Department of Pharmaceutical Science; [3]Department of Chemical Sciences; [4]Department of Life Science; University of Trieste; Trieste, Italy; [5]Optical Imaging Laboratory; CBM; Area Science Park; Trieste, Italy;

[†]These authours contributed equally to this work.

Key words: PDT, PEGylated pheophorbide *a*, phototoxicity, biodistribution, in vivo imaging

The design of new photosensitizers with enhanced phototoxicity and pharmacokinetic properties remains a central challenge for cancer photodynamic therapy (PDT). In this study, Pheophorbide *a* (Pb*a*) has been pegylated to methoxypolyethylene glycol (mPEG-Pb*a*) to produce a soluble photosensitizer that exhibits a higher tissue distribution than free Pb*a*. In vitro studies have shown that mPEG-Pb*a* promotes a fairly strong photosensitizing effect in cancer cells, as previously observed for the unpegylated molecule. mPEG-Pb*a* targets the mitochondria where, following photoactivation, ROS are produced which cause a cellular injury by lipid peroxidation. The effect of pegylation on the photosensitizer biodistribution has been examined in different selected organs of female mice, at different time points after intraperitoneal administration of the drug (50 μmol/Kg body weight). Other than free Pb*a*, which showed a low tissue accumulation, mPEG-Pb*a* has been detected in significant amounts (8 to 16 μg/ml) in liver, spleen, duodenum and kidney and, 3–5 hours after intraperitoneal injection, in moderate amounts (3 to 8 μg/ml) in brain and lung. In vivo optical imaging performed on living female C57/BL6 mice bearing a subcutaneous melanoma mass, showed that injected mPEG-Pb*a* distributes all over the body, with an higher uptake in the tumor respect to free Pb*a*. Our results indicate that although pegylation somewhat decreases the phototoxicity, it significantly increases the drug solubility and tissue distribution and tumor uptake of mPEG-Pb*a*, making the conjugate an interesting photosensitizer for PDT

Introduction

Photodynamic therapy (PDT) is a non-invasive therapeutic modality used in a number of diseases including psoriasis, age-related macular degeneration and cancer.[1-6] It involves the systemic or topic administration of a photosensitizer, followed by irradiation with light. The activated photosensitizer converts oxygen to singlet oxygen and/or reactive oxygen species (ROS) which lead to cell death and tissue necrosis. One aim of PDT research is the discovery of new photosensitizers possessing minimal dark cytotoxicity, high photodynamic properties, improved pharmacokinetics, preferential retention in diseased instead of healthy tissues, chemical stability and a good cellular uptake.[7-9] Though a number of new phosensitizers have been proposed, the most widely used in clinic is a mixture of hematoporphyrines (Photofrin®). It is used for different cancers, but its absorption above 600 nm[10] is weak, so there is great interest to search for new and more efficient PDT molecules. We recently focused our efforts on pheophorbide *a* (Pb*a*), a chlorophyll derivative. Compared to Photofrin, Pb*a* is characterized by a stronger absorption between 650–700 nm, in the tissue-penetrating wavelength range. We found recently that Pb*a*, irradiated at 14 J/cm^2, induces a potent photodynamic effect in different cancer cells with IC_{50} values between 70 and 250 nM.[11] The intracellular target of Pb*a* was found to be mitochondria membranes, where it activates a peroxidation process which eventually causes cell death by apoptosis and/or necrosis.[11,12] The photodynamic activity of Pb*a* have been studied in cultured cells by several authors.[11-16] Furthermore, Tang et al.[17] have reported that photoactivated Pb*a* downregulates the expression of P-glycoprotein and inhibits the multidrug resistance activity in human hepatoma cells. There are only few in vivo studies of PDT with Pb*a* as a photosensitizer. Hajri et al.[16,18] showed that animal doses of 30 mg/Kg of liposome/Pb*a* combined with light at the fluence of 100 J/cm^2 reduce the growth of HT29 xenografts of human colon adenocarcinoma. Xenografts of human hepatoma (HepG3b cells) treated with Pb*a* (intravenous dose of 0.3 mg/Kg) and light at a fluence of 126 J/cm^2, significantly reduced the tumor volume by more

*Correspondence to: Luigi E. Xodo; Email: luigi.xodo@uniud.it
Submitted: 02/12/10; Revised: 05/27/10; Accepted: 05/31/10
Previously published online: www.landesbioscience.com/journals/cbt/article/12536
DOI:10.4161/cbt.10.5.12536

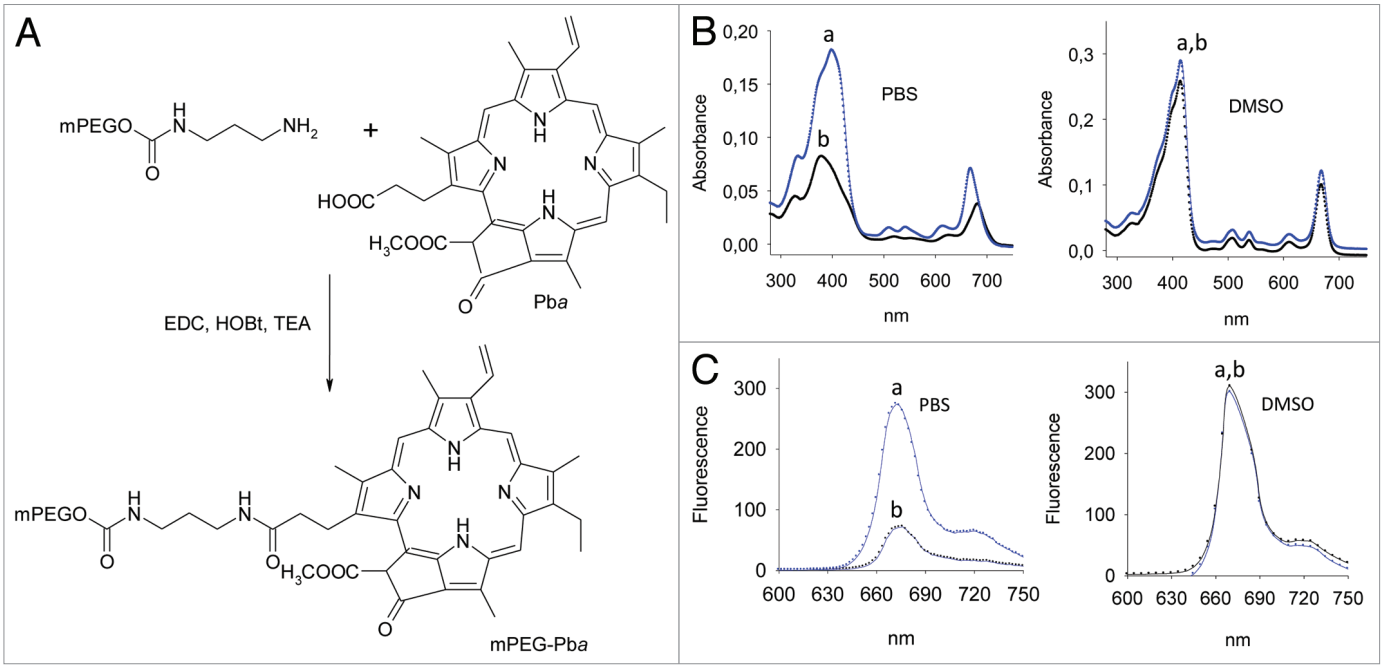

Figure 1. (A) Structure of Pheophorbide *a* and its conjugation of methoxy polyethylene glycol. (B) Absorption spectra of mPEG-Pb*a* (a) and Pb*a* (b) (5 μM) in PBS and DMSO, cuvette pathlength 1 cm; (C) fluorescence spectra of mPEG-Pb*a* (a) and Pb*a* (b) (1 μM) in PBS and DMSO. Flourescence spectra were obtained with a microplate fluorometer, Ex. 400 nm.

than 50%. Evrard et al.[19] reported the potential of Pheophorbide *a* as photosensitizer to treat azaserine-induced pancreatic rat carcinoma. A dose of 9 mg/Kg i.v., and light treatment at 100 J/cm^2 induced selective necrosis of the tumor. Six of nine rats were cured in 120 days whereas all 36 control animals died within 35 days. For in vivo applications the capacity of the photosensitiser to reach in the diseased tissues becomes critical, in particular when a large peritoneal area is interested as occurring in carcinomatosis and sarcomatosis. To improve the pharmacokinetics of the photosensitizer we pegylated Pb*a* to polyethylene glycol (PEG), as PEGylation has proved to be a valid technology to transform proteins, peptides, small molecules and oligonucleotides into more potent drugs than their respective unconjugated analogues.[20] PEGylated drugs, with respect to their unmodified analogues, show more useful clinical properties such as increased stability and solubility,[21] reduced renal clearance,[20] longer circulating half-life,[22,23] reduced immunogenicity and improved selectivity against tumor tissues.[24,25] In this work we investigated two important aspect of PEGylation. First, we asked whether PEGylated Pb*a* is an equally potent photosensitizer as free Pb*a* and whether free or pegylated Pb*a* mediates the same type of response in cancer cells after light activation. Second, we investigated in vivo whether PEGylation improved the tissue distribution of the photosensitizer and its tumor uptake.

Results and Discussion

PEGylated Pb*a*. The synthesis of monoethoxy polyethylene glycol (mPEG) was carried out according to **Figure 1A**, while its fluorescent derivative was prepared following a new procedure, based on orthogonally protected amino-derivatives of commercial diOH-PEG, modified with linkers bearing differently reactive terminal amino groups, which was recently developed and patented.[26] Once obtained this selectively end-modified polymer derivative, fluorescein was coupled to the free NH_2 carried by the 1,3-diaminopropane linker. Successively, the deprotection of the second amino group from Z by catalytic hydrogenation allows the final conjugation of the Pb*a* molecule through an amido bond. We also obtained the fluoresceinated derivative of mPEG-Pb*a* (Fluo-PEG-Pb*a*), as described in the experimental section.

Two major advantages we expected from PEGylation: an increase of photosensitizer solubility in water and a slower rate of elimination from the body.

The absorption spectra of free and pegylated Pb*a* (mPEG-Pb*a*) in PBS are shown in **Figure 1B**. At the same concentration (5 μM), Pb*a* shows absorption bands of lower intensity, as a result of aggregation, whereas in DMSO the bands are identical. The fluorescence spectra of Pb*a* and mPEG-Pb*a* are reported in **Figure 1C** (Ex. 400 nm). In DMSO, the fluorescence spectra are indistinguishable, while in PBS the fluorescence quantum yield of free Pb*a* is about 3/4-fold lower than that of mPEG-Pb*a*.

Photocytotoxicity of mPEG-Pb*a*. The photocytotoxicity of mPEG-Pb*a* was evaluated in four cancer cell lines: HeLa, $HepG_2$, MCF-7 and B78-H1. This was done by a dose-response experiment where the cells were treated with increasing amounts of mPEG-Pb*a*, illuminated with a halogen lamp at the fluence of 14 J/cm^2, analysed by a standard resazurin assay, 24 h later. The photosensitizer was added to the cell medium without using any transfecting agent. Under these conditions, mPEG-Pb*a* showed IC_{50} values between 200 and 1,200 nM: 650 nM (HeLa), 300 nM

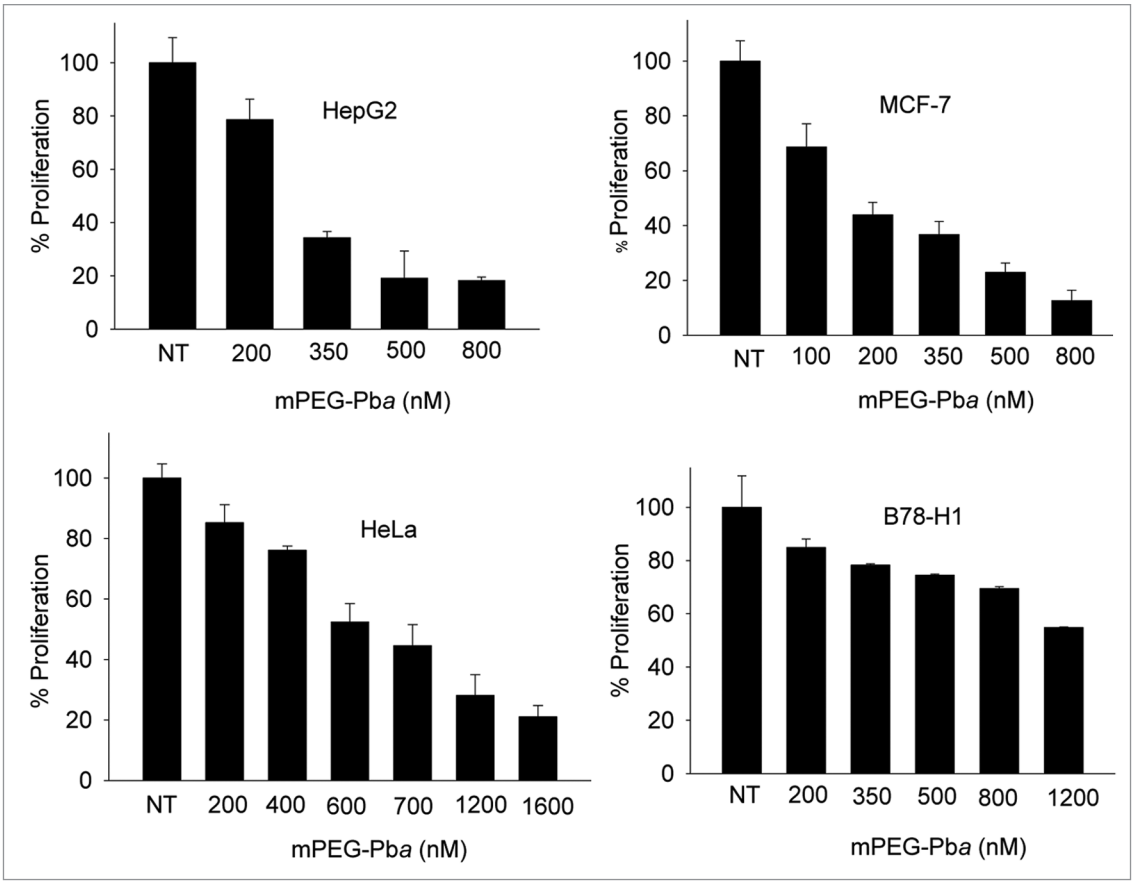

Figure 2. Dose-response experiment in which cancer cells have been treated with increasing amounts of mPEG-Pb*a*, irradiated with halogen lamp at 14 J/cm^2. 24 h following irradiation a standard resazurin assay was performed. The values reported are the average of three independent experiments.

(HepG2), 200 nM (MCF-7) and 1,200 nM (B78-H1) (**Fig. 2**). These values are from 3- to 5-fold higher than those obtained for unconjugated Pb*a* (**Table 1**), but mPEG-Pb*a* may still be considered a good photosensitizer. The difference of the IC_{50} values can be explained in terms of increased quantum yield of fluorescence of mPEG-Pb*a* compared to Pb*a*, observed in aqueous solution. It is firmly established that the quantum yield of a photosensitizer is given by the quantum yield of singlet oxygen generation (Φ_Δ) and of the quantum yield of fluorescence (Φ_{FL}), $\Phi_\Delta + \Phi_{FL} = 1$. For free Pb*a*, Φ_Δ is relatively high and Φ_{FL} relatively low, driving its photodynamic potential.[27] As described by Röder and co-workers $\Phi_\Delta + \Phi_{FL} = \Phi_{ISC} + \Phi_{IC} + \Phi_{FL} = 0.64 + 0.08 + 0.28 = 1$, where Φ_{ISC} is the Φ_{IC} are the quantum yields of intersystem crossing and internal conversion, respectively.[27] This gives relatively low fluorescence, as observed in the current study with basic Pb*a*, and high photodynamic activity.[11-16] With mPEG-Pb*a* we observed an increase in the fluorescence (in aqueous solution) and a decrease in cytotoxicity, as determined from the IC_{50} values reported **Table 1**. So, the change of Φ_{FL} (and of Φ_Δ) explain the finding that pegylation causes a loss of IC_{50} and gain of fluorescence.

The lower phototoxicity mPEG-Pb*a* may also reflect a different cellular uptake between the two forms of the photosensitizer. Following a method previously described,[28] we treated for 3 h HeLa/HepG2 cells with 160 nM Pb*a*/mPEG-Pb*a* and measured the photosensitizer fluorescence in the lysate (Ex = 400 nm; Em = 670 nm). We found that despite Pb*a* has a Φ_{FL} lower than mPEG-Pb*a*, it gave a signal 5-fold higher than mPEG-Pb*a*, indicating that the former enters into the cells more efficiently than the latter (not shown). This does not come as a surprise because the uptake of polymer-conjugated drugs normally occurs by endocytosis, while small molecules by passive diffusion.[25]

Table 1. IC_{50} values for Pb*a* and mPEG-Pb*a* in four cancer cells

Cell lines	IC_{50} (nM) Pb*a*	IC_{50} (nM) mPEG-Pb*a*
HeLa Human cervical cancer cells	140 ± 20	650 ± 20
HepG2 Human hepatocarcinoma cells	95 ± 5	300 ± 20
MCF-7 Human breast adenocarcinoma cells	65 ± 5	250 ± 10
B78-H1 Murine amelanotic melanoma cells	250 ± 20	1200 ± 30

We also found that in the dark mPEG-Pb*a* is not cytotoxic over a period of 72 h, at the concentration of 1,600 nM (data not shown).

Photokilling mechanim. The photokilling mechanism triggered by photoactivated mPEG-Pb*a* was investigated in HepG2 and HeLa cells. First, we addressed the question whether upon photoactivation mPEG-Pb*a* produces ROS, in the presence of oxygen. A standard CM-H_2DCFDA assay on HeLa cells was

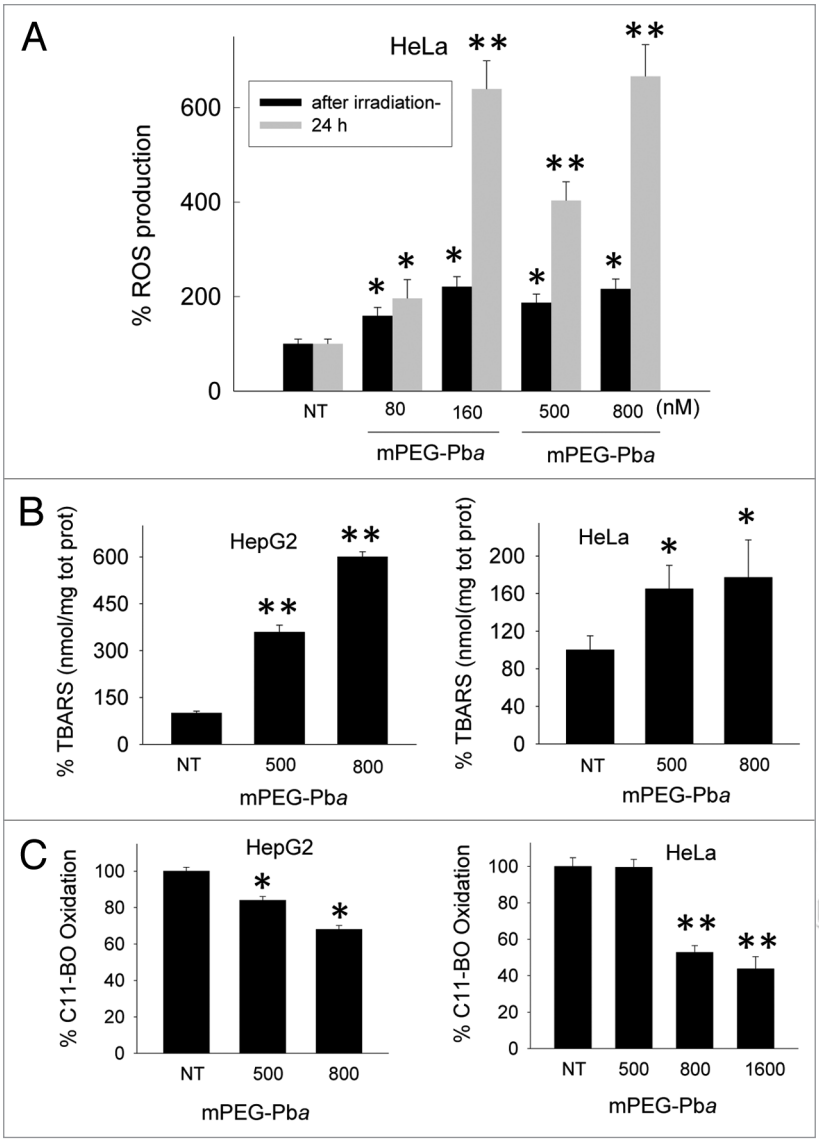

Figure 3. (A) Fluorescence measured by cell cytometry of HeLa cells treated for 3 h with Pb*a* and mPEG-Pb*a*, activated by light and then after light activation or after 24 h treated with 10 µM CM-H_2DCFDA. The increase of fluorescence is proportional to the ROS generation. The photosensitizer concentrations used have been chosen near to IC_{50} values. (B) Lipid peroxidation detected by TBARS. Levels of TBA reactive species (nmol/mg total protein) in HepG2 and HeLa cells. Assay performed 24 h following mPEG-Pb*a* photoactivation. (C) Oxidation of C11-BODIPY$^{581\text{-}591}$ in HepG2 and HeLa cells. Assay performed 24 h following mPEG-Pb*a*/light treatment. Fluorescence measured with a microplate reader (Exc 591, Em 635). Values represent the relative red fluorescence decay. Standard t-test versus control (NT): *$p < 0.05$; **$p < 0.01$.

carried out. This assay is based on the observation that the dye in its reduced form is not fluorescent, but it becomes so when it is oxidized by ROS and the dye acetate groups are removed by cellular esterases. The amount of fluorescence generated in the cells by this transformation was measured by FACS. **Figure 3A** shows that both Pb*a* or mPEG-Pb*a* efficiently generate ROS in HeLa cells. In order to see if the generated ROS attacked the integrity of the cell membranes, the level of lipid peroxidation was measured by means of a TBARS assay.[29] In this assay the presence of malonyldialdhyde (MDA, product of lipid peroxidation) bound to thiobarbituric acid (TBA) is measured by spectrofluorimetric experiments. In untreated cells, the level of the TBARS is relatively low and set to 100 (control). In mPEG-Pb*a* treated and photoactivated cells, the level of this adduct increases proportionally to the photosensitizer concentration: up to 6-fold in HepG2 cells, nearly 2-fold in HeLa cells, as previously observed with unconjugated Pb*a*[11] (**Fig. 3B**). This demonstrates that photoactivated mPEG-Pb*a* promotes lipid peroxidation, which appears particularly strong in HepG2 cells, as these are more sensitive to mPEG-Pb*a* than HeLa cells (**Table 1**). Further evidence of lipid peroxidation by mPEG-Pb*a* was obtained by measuring the oxidation of the C11 BODIPY$^{581/591}$ dye by the peroxyl radicals generated by photoactivated mPEG-Pb*a*. **Figure 3C** shows that mPEG-Pb*a* reduces the dye fluorescence at 595 nm in a dose-response way, a behavior indicative of lipid peroxidation.[30-32]

Next, we addressed the question of what the cellular target of mPEG-Pb*a* is. A first indication that mPEG-Pb*a* targets the mitochondria was obtained by confocal microscopy in HeLa and HepG2 cells treated with mPEG-Pb*a* conjugated to fluorescein (Fluo-PEG-Pb*a*) and MitoTracker red, a dye specific for mitochondria. Typical images obtained with HepG2 cells show that MitoTracker (red staining) colocalizes with Fluo-PEG-Pb*a* (green fluorescence) (**Fig. 4**). Combining the results of the TBARS assay with the confocal microscopy data, it could be concluded that photoactivated mPEG-Pb*a* causes a membrane injury involving the mitochondria. This was confirmed by measuring in HeLa cells the membrane potential of the mitochondria by a JC-1 assay[33] (**Fig. 5**). The cells were treated with increasing amounts of mPEG-Pb*a* (500, 800 and 1,600 nM), and analysed by FACS in the presence of JC-1. It can be seen that the percentage of cells with a depolarized membrane raised from 5.42% (untreated cells) to 66% (treated cells), indicating that mPEG-Pb*a* induced, a mitochondria membrane depolarization, as observed with free Pb*a*.[11,12]

Finally, the effect of mPEG-Pb*a* on the cell cycle was analyzed on HeLa and HepG2 cells by FACS. The data obtained are summarized in **Table 2**. It can be seen that mPEG-Pb*a*, 500 and 800 nM, arrests the cell cycle in both cell lines, as indicated by a strong increase of the G_2/M phase at 24 h following light treatment. This is observed also at 48 and 72 h in HepG2 cells, whereas in Hela cells the cell cycle arrest weakens with time. In accord with this finding, proliferation data showed a rescue of growth by HeLa cells (S_1), confirmed by the fact that the S-phase increased at both doses of mPEG-Pba (500 and 800 nM). Conversely, with HepG2 cells we observed a cell growth

rescue only at the dose of 500 nM, as with 800 nM mPEG-Pb*a* the arrest is complete. The presence of a preG1 peak indicates that a fraction of cells is either apoptotic or necrotic. Indeed, both cell lines showed an increase of caspase at 2 h after light treatment, indicating that a fraction of cells dies by apoptosis and, according to time lapse imaging (S_2), also by necrosis.

In vitro and in vivo studies of Pb*a* and mPEG-Pb*a*. The in vitro cellular studies showed that mPEG-Pb*a*, having IC_{50} values between 250 and 1,200 nM, can be considered a strong photosensitizer, although its phototoxicity is a bit lower than that of free Pb*a*.[11] We therefore focused on in vivo biodistribution studies. To know if mPEG-Pb*a* is hydrolytically stable in aqueous solution—a property required to antitumoral PDT drugs—we performed a stability study. The PEG moiety is linked to Pb*a* via an amide bond. Although this bond is relatively stable (the order of stability to hydrolysis is ether > amide > ester), we checked whether mPEG-Pb*a* undergoes hydrolysis under physiological conditions. We determined by HPLC the amount of Pb*a* released by PEG-Pb*a* dissolved in PBS (pH 7.4, 37°C),[34] over an interval of 24 h and found that the amount of Pb*a* released was about 2%, thus suggesting that the conjugate was hydrolytically stable in PBS.

Next we performed a pharmacokinetic study to determine the biodistribution of Pb*a* and mPEG-Pb*a*, following 50 µmol/Kg i.p. injection in female C57/BL6 mice. Pb*a* is insoluble in water but it dissolves in 10% DMSO saline solution. The animals were sacrificed at different time points varying between 1 and 24 h (six mice not injected at time 0 and four mice injected at each time point). Brain, kidney, duodenum, spleen, lung and liver were removed and homogenized in MeOH-DMSO (4 + 1 v/v). These homogenates were centrifuged and the amount of Pb*a* or mPEG-Pb*a* present in the supernatant was measured by fluorescence (Ex. 409 nm, Em. 676 nm).[35] No interference from other compounds present in the extracts was observed. **Figure 6A** shows that only the brain extract from the mouse treated with mPEG-Pb*a* shows emission at 676 nm, while the brain extract from untreated mice does not. The amount of Pb*a* or mPEG-Pb*a* present in the various organs was determined by means of a calibration curve, obtained by plotting fluorescence intensity against Pb*a* or mPEG-Pb*a* concentrations using standard calibration photosensitizer solutions. The curves were linear in the range 0.5–25 µg/ml with a correlation coefficient (r^2) close to 0.99. The data reported

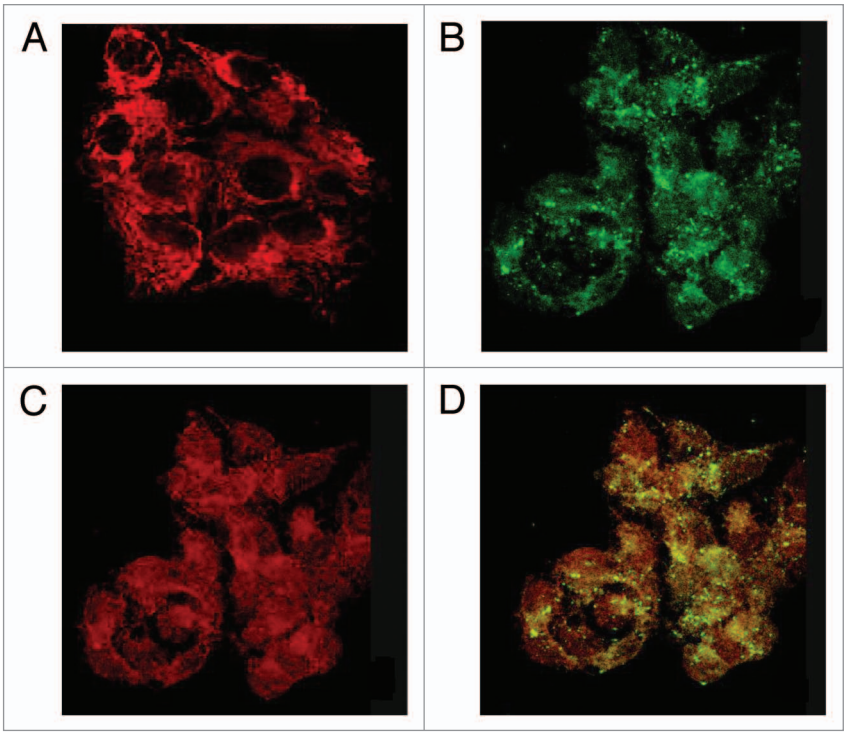

Figure 4. (A) Confocal microscopy images of HepG2 cells treated with only MitoTracker (control); (B–D) HepG2 cells photodynamically treated with Fluo-PEG-Pb*a* and MitoTracker (added after light treatment): fluorescence emitted by Fluo-PEG-Pb*a* is shown in part (B); fluorescence emitted by MitoTracker is shown in part (C); merge of parts B and C (D).

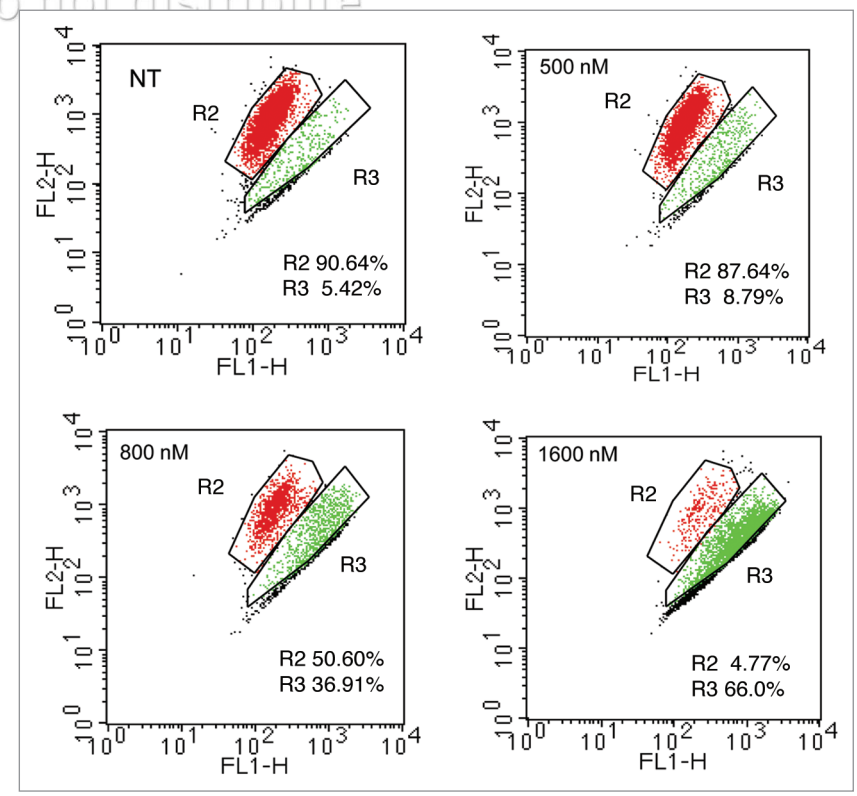

Figure 5. mPEG-Pb*a* (500, 800 and 1,600 nM) treated HeLa cells, stained with JC-1 24 h after light treatment and analyzed by cell cytometry.

Table 2. Cell cycle analysis of HeLa and HepG2 cells photodynamically treated with mPEG-Pb*a*

	Cell Cycle	24 h	48 h	72 h
Control (HeLa)	Sub-G_1	0.01	3.56	4.2
	G_0/G_1	65.2	64.3	64.0
	S	29.1	25.9	25.1
	G_2/M	5.69	6.24	6.7
mPEG-Pb*a* 500 nM (HeLa)	Sub-G_1	6.0	7.4	7.8
	G_0/G_1	42.8	47.1	56.1
	S	19.0	22.0	24.0
	G_2/M	32.2	23.5	12.1
mPEG-Pb*a* 800 nM (HeLa)	Sub-G_1	7.2	8.3	10.5
	G_0/G_1	43.6	45.2	48.8
	S	18.2	19.0	21.5
	G_2/M	31.0	27.5	19.2
Control (HepG2)	Sub-G_1	0	5.9	0
	G_0/G_1	66.0	65.6	66.9
	S	12.0	13.0	15.0
	G_2/M	22.0	15.1	17.8
mPEG-Pb*a* 500 nM (HepG2)	Sub-G_1	1.1	2.5	2
	G_0/G_1	53.1	54.1	56.2
	S	6.4	8.4	11.0
	G_2/M	39.4	35.0	30.1
mPEG-Pb*a* 800 nM (HepG2)	Sub-G_1	14.9	15.9	14.4
	G_0/G_1	41.1	39.1	41.5
	S	5.4	4.3	3.6
	G_2/M	38.5	41.6	40.5

in **Figure 6B** show that: (i) the administration of the mPEG-Pb*a* either in saline solution (sol 1) or saline solution-DMSO (9 + 1, v/v) (sol 2) give the same tissue distribution; (ii) PEGylation has a dramatic impact on the tissue distribution of the photosensitizer; in all organs analyzed, mPEG-Pb*a* is from 8- to 13-fold more concentrated than free Pb*a*; (iii) the main targets for mPEG-Pb*a* 24 h post-injection are the following: kidney > liver > spleen > intestine > lung > brain; (iv) free Pb*a* was present in the various organs in non-significant amounts, 24 h post injection. Some Pb*a* was detected only in liver and duodenum at 3 h post injection (**Fig. 6C**).

It can be seen that there is a clear urinary output of mPEG-Pb*a* not observed for native Pb*a* which is cleared by the bile, recycled in blood and liver with an entero-hepatic cycle and eliminated in the stools.[36] The persistence of mPEG-Pb*a* in the liver and the duodenum (**Fig. 6C**) and the delayed urinary output of this water-soluble drug suggest the coexistence of bile clearance and blood recycle for this conjugate.

Time domain optical in vivo imaging allows longitudinal animal studies to evaluate the time biodistribution of Pb*a* and mPEG-Pb*a* in the same animal up to 48 h. **Figure** 7 shows a typical time domain analysis of mice injected with equal amounts (50 µmol drug/Kg) of Pb*a* or mPEG-Pb*a***.** It can be seen that mPEG-Pb*a* is found widely distributed in the whole body of the animal at 1 h post injection, whereas free Pb*a* does not, as it appears located mainly in the peritoneal region, in a lower amount according to signal intensity. At 3 and 5 h post injection, mPEG-Pb*a* shows the maximum tissue distribution, which, though in lower amounts as indicated by the weakening of the fluorescence signal, persists up to 24 and 48 h. For a correct comparison between the two photosensitizers, one should consider that the Φ_{FL} of mPEG-Pb*a* is higher than the Φ_{FL} of Pb*a*. This difference is significant in aqueous solution (see **Fig. 1C**) but it is likely to be much lower in a cellular environment (the targets of Pb*a* are the membranes in which the molecule is not aggregated).[27] The imaging data demonstrate that PEGylation improves the tissue distribution of the photosensitizer, suggesting that mPEG-Pb*a* should be more suitable for in vivo application than free Pb*a*.

We also investigated whether mPEG-Pb*a* accumulates in a tumor mass more than free Pb*a*. To this aim four mice have been subcutaneously inoculated with 1 x 10^6 murine amelanotic melanoma cells to induce the formation of a tumor mass. Two mice were allowed to develop a subcutaneous small tumor mass (5–10 mm^3) before imaging, while the other were let to grow a larger tumor mass (30–35 mm^3). The mice bearing the tumor have been injected intraperitoneally with 250 µl of Pb*a* or mPEG-Pb*a* solution (50 µmol drug/Kg) and subjected to a whole body scan at increasing post-injection times from 1 to 48 h (S_3). At 48 h post injection the mice were sacrificed in order to perform ex vivo analysis on the main organs and tumor for both free and pegylated Pb*a* at the same dose. Interestingly, the uptake of the tumor is higher than that of the various organs (**Fig. 8A and B**). With mPEG-Pba the order of uptake is: tumor > kidney > liver > intestine > lung (no drug in brain and spleen); while with Pb*a* the order is: tumor > intestine > liver > kidney (no drug in brain, spleen, lung). **Figure 8C** shows a direct comparison between tumor uptake observed with free and pegylated Pb*a*. When the same amount of drug is delivered to the mice, it is found that both small and large tumors take up more mPEG-Pb*a* than free Pb*a*: the intensity of the fluorescence emitted by mPEG-Pb*a* is roughly 3-fold higher than that observed with free Pb*a*.

It is noteworthy that the distribution data obtained by fluorescence analysis of homogenized organs (**Fig. 6B and C**) is apparently not in full accord with the imaging data. This may be due to the different sensibility of the two methods. However, excluding the tumor, both analyses indicate the intestine as the main target for Pb*a*, whereas the kidney is the main target for mPEG-Pb*a*. This is likely due to: (i) a bile clearance for Pb*a* and a combined bile clearance and blood recycle for mPEG-Pb*a*; (ii) the fact that the photosensitizers were injected in the peritoneal region and that mPEG-Pb*a* diffuses into the body more rapidly than Pb*a*.

Conclusion

The data of this study show that mPEG-Pb*a* is a soluble and promising photosensitizer for PDT. Upon irradiation at 14 J/cm^2, mPEG-Pb*a* shows IC_{50} values between 250 to 1,200 nM in

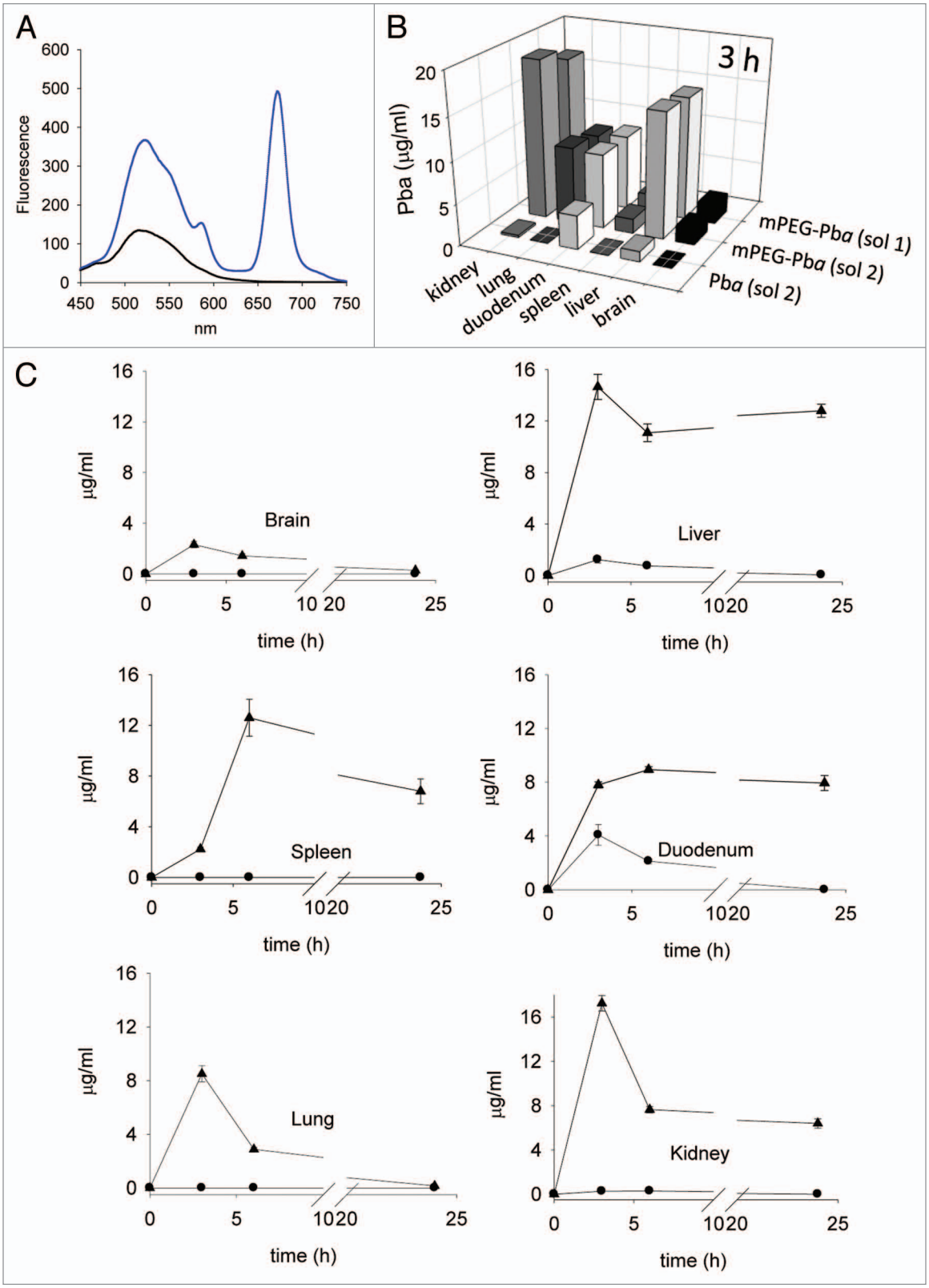

Figure 6. (A) Fluorescence emission spectra of mouse tissue brain extract obtained from mice non injected (blank) or injected with mPEG-Pb*a*. Ex = 409 nm, Em = 670 nm. (B) Tissue distribution of photosensitizer Pb*a* and mPEG-Pb*a* as a function of time, obtained from mice i.p. injected with the drugs. The photosensitizer has been injected in mice with a saline solution (sol 1), saline solution-DMSO (9 + 1, v/v) (sol 2). (C) Amounts of photosensitizer found in the various tissues. Symbols: mPEG-Pb*a* (▲); Pb*a* (●). Each point is the average of values obtained with four mice.

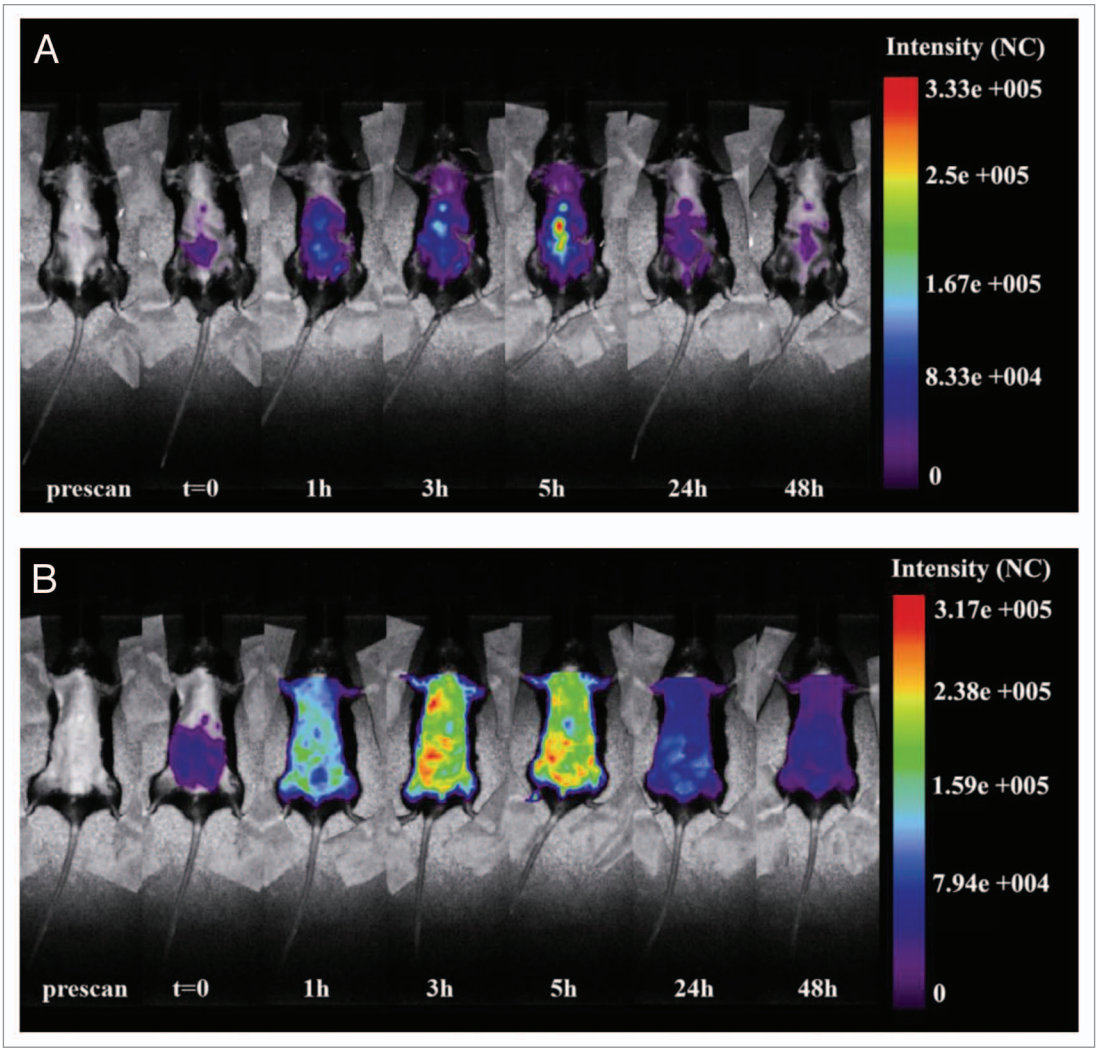

Figure 7. In vivo time domain optical images of mice treated with Pb*a* or mPEG-Pb*a*. Biodistribution of Pb*a* (A) and mPEG-Pb*a* (B) in mice after i.p. injection. Whole body fluorescence intensity was acquired at indicated times following post-injection. Images corresponding to two different experiments for each pheophorbide formulation are reported.

the four tested cell lines. In the dark the drug is not cytotoxic at PDT concentrations, but when it is photoactivated it produces ROS that cause membrane injury marked by an increase of malonyldialdheyde and a depolarization of mitochondria membranes: cellular events that lead to cell death primarily by necrosis. When the conjugate is intraperitoneally injected in mice, a significant amount of it reaches the main tissues of the body other than the unconjugated analogue, which shows a very poor bio-distribution. The solubility and phototoxicity of mPEG-Pb*a* suggest it may be a good photosensitizer for PDT, but also because the drug shows a urinary output with a relatively quicker elimination than native Pb*a*, with a consequent lower risk of skin and mucosa phototoxicity.

This significant increase of the tissue distribution caused by PEGylation has also been confirmed by time domain optical in vivo imaging. PEGylated Pb*a* maintains the photodynamic properties of the free drug but shows an improved biodistribution, which makes the conjugate a promising PDT drug for cancer therapy.

Material and Methods

Materials. mPEG-OH (MW = 5,000 Da), 1,3-diaminopropane, N,N'-disuccinimidyl carbonate (DSC), N-(3-dimethylaminopropyl)-N-ethyl carbodiimide (EDC) and 1-hydroxybenzotriazole (HOBT) were purchased from Fluka (Buchs, Switzerland). Pb*a* (MW 592.69) was purchased from Frontier Scientific (Logan, Utah). Fluorescein-N-hydroxysuccinnimido (Fluo-NHS) was obtained from Aldrich (Milan, Italy). The synthesis of mPEG-NH_2 and of Z-PEG-NH_2 (M.W. = 5,000 Da) was carried out following the procedures previously described.[37]

Synthesis of mPEG-Pb*a*. Pb*a* (5 eq) was dissolved in the minimum amount of anhydrous CH_2Cl_2 and, whilst stirring, 5 eq each of HOBT, EDC and TEA were added in this order. The resulting solution was added to monomethoxy PEG-NH_2 (1 eq) dissolved in anhydrous CH_2Cl_2. The reaction was left stirring overnight at room temperature. The product was precipitated

by slow addition, in ice-bath of diethyl ether. It was filtered, recrystallized from EtOH and dried over KOH pellets under vacuum (yield 97%).

^{1}H NMR (DMSO-d_6) δ, ppm: 9.78 (s, 1H, meso-H), 9.45 (s, 1H, meso-H), 8.91 (s, 1H, meso-H), 8.21 (m, 1H, C<u>H</u>=CH_2), 7.61 (m, 1H, N<u>H</u>-CO), 7.05 (m, 1H, N<u>H</u>-COO), 6.41 (s, 1H, C<u>H</u>-$COOCH_3$), 6.30 (dd, 2H, CH=C<u>H_2</u>), 4.55 (m, 1H, C<u>H</u>-CH_3), 3.98 (m, 3H, C<u>H_2</u>-OCONH + C<u>H</u>-$(CH_2)_2$-COOH), 3.53–3.32 (m, 454H, PEG), 2.83 (m, 4H, C<u>H_2</u>-CH_2-C<u>H_2</u>), 2.20 (m, 2H, C<u>H_2</u>-CH_2-COOH), 1.95 (m, 2H, CH_2-C<u>H_2</u>-COOH), 1.76 (d, 3H, C<u>H_3</u>-CH), 1.61 (t, 3H, C<u>H_3</u>-CH_2-), 1.49 (m, 2H, CH_2-C<u>H_2</u>-CH_2).

Synthesis of Fluo-PEG-Pb*a*. (a) Fluo-PEG-Z: Z-PEG-NH_2 (M.W. = 5.000 Da, 100 mg, 0.02 mmol) was coevaporated with anhydrous CH_2Cl_2 (x2) and dried using a rotary pump; the product was dissolved in the minimum quantity of anhydrous CH_2Cl_2 and reacted with 7 eq of Fluo-NHS (78 mg, 0.14 mmol). The system was left under stirring for 18 h at room temperature. The product mixture was precipitated by Et_2O in an ice-bath, filtered and recrystallised from EtOH. Yield 94%; (b) Fluo-PEG-NH_2: Z-PEG-Fluo (100 mg) was dissolved in MeOH in a three-neck 50 ml flask, 10% Pd/C was added as catalyst in a quantity equal to 10% by weight on the substrate and the suspension was brought to pH 3 by slowly adding few drops of concentrated HCl. The system was left under stirring overnight under H_2 atmosphere and room temperature. After removing the catalyst by filtration, the MeOH was evaporated under reduced pressure. The solid obtained was dissolved in CH_3CN and precipitated with Et_2O in an ice-bath, filtered, washed with Et_2O and stored over KOH pellets. Yield 90%; (c) Fluo-PEG-Pb*a*: 5 equivalents of Pb*a* were dissolved in the minimum amount of anhydrous CH_2Cl_2 and whilst stirring 5 equivalents each of HOBT, EDC and TEA were added in this order. This solution was added to the Fluo-PEG-NH_2 (1 eq) dissolved in anhydrous CH_2Cl_2. The reaction was left stirring at room temperature overnight. The product was precipitated by slow addition, in an ice-bath of diethyl ether. It was then filtered, recrystallised from EtOH and dried over KOH pellets under vacuum. Yield 97%. The purity of the PEGylated derivatives was verified by HPLC and their identity was confirmed by UV, Fluorescence and 1H-NMR analysis (S_4).

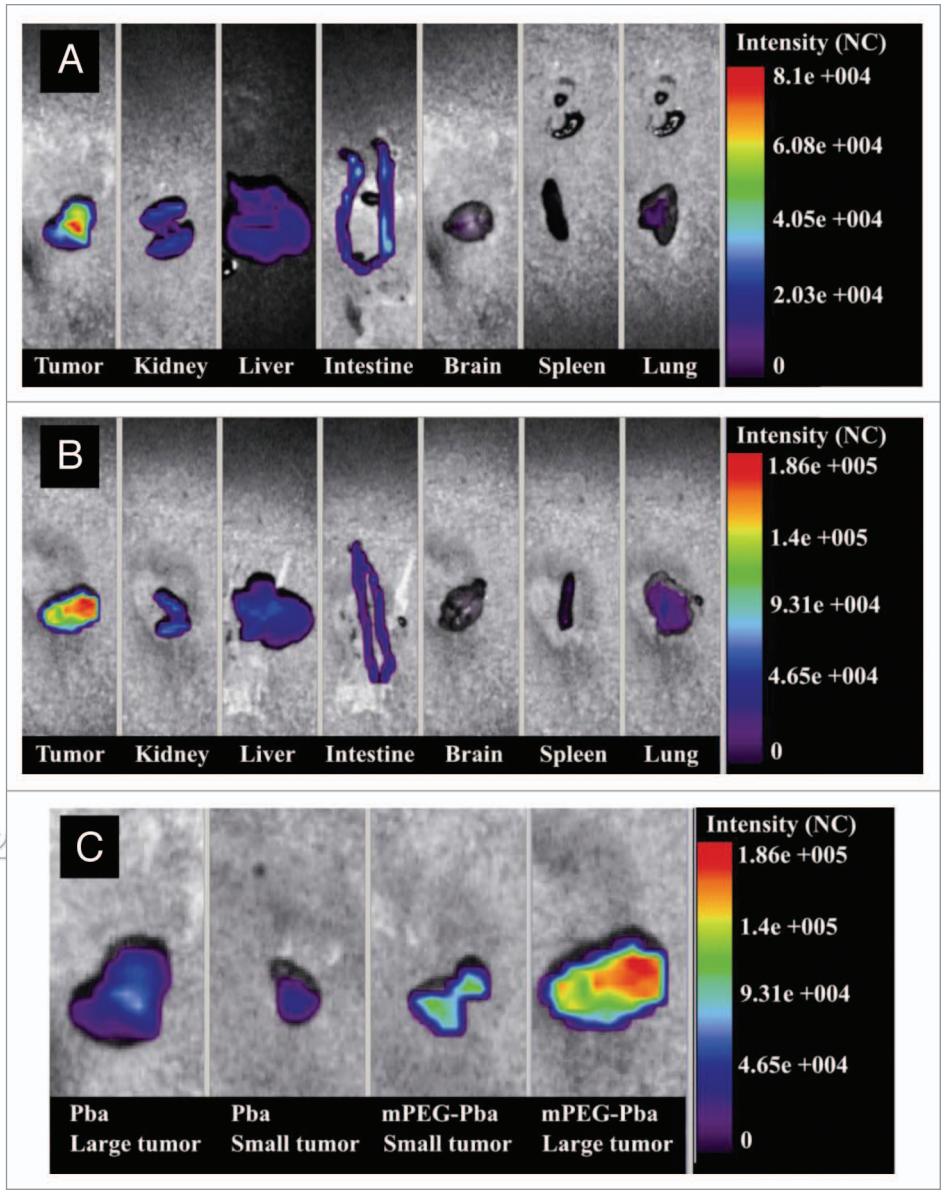

Figure 8. Ex vivo images of organs obtained from mice bearing a tumor, 48 h following i.p. injection of 250 µl of Pb*a* or mPEG-Pba solution (50 µmol/Kg). (A) mouse treated with Pba; (B) mouse treated with mPEG-Pba. (C) Comparison of tumor uptake (large and small tumor mass) of Pb*a* and mPEG-Pb*a*. The analyses A–C are independent in terms of laser intensity and signal integration time. Experiment was carried out in duplicate.

Cell lines. HeLa human cervical cancer and HepG2 hepatic carcinoma cells were cultured in DMEM; MCF-7 human breast cancer cells were cultured in RPMI and B78-H1 amelanotic derived from murine melanoma cells were cultured in DMEM. All media contained 10% fetal calf serum and were supplemented with antibiotics Penicillin 100 U/ml, Streptomycin 100 µg/ml and Glutamine 2 mM (CELBIO, Milan, Italy).

PDT treatment. Pb*a* and mPEG-Pb*a* were dissolved in DMSO and conserved in aliquots of 0.5 mM at -80°C. The stability in aqueous solution of Pb*a* and mPEG-Pb*a* were checked by

measuring the UV-vis spectrum at intervals of weeks. The cells were treated with the photosensitizer in the dark for 3 hours, then irradiated with metal halogen lamp at an irradiance of 8 mW/cm^2 for 30 min (~14 J/cm^2).

Proliferation assay. The percentage of viable cells 24 h after light activation was determined by the resazurin assay following the manufacturer's instructions (Sigma- Aldrich, Milan, Italy). The values were obtained by spectrofluorometer Spectra Max Gemini XS (Molecular Devices, Sunnyvale, California 94089). The cells were seeded in a 96-multiwell plate: HeLa, 5,000 cells/well; HepG2, 7,000 cells/well; MCF-7, 7,000 cell/well and B78-H1, 5,000 cells/well.

Propidium iodide staining and FACS analysis. Cell cycle analyses were performed in HeLa and HepG2 cells after PDT treatment. Briefly, HeLa and HepG2 cells were seeded in a 6-well plate at a cell density of 2 x 10^5 cells/well, 24 h before PDT treatment. Following light treatment the cells were harvested at different times, re-suspended in 0.5 ml of PBS and washed twice. Under vortexing, 1 ml of ice-cold 70% ethanol was added dropwise to the pellet and the cells were allowed to fix overnight at 4°C. After centrifugation prior to FACS analysis the cells were stained with a 0.5 ml solution containing 0.05 mg/ml propidium iodide and 0.5 mg/ml RNase A, incubated for 30 min at 37°C and then analysed by FACScan (Becton Dickinson, San Jose, USA), using Win MDI 2.8 software.

ROS measurement. ROS levels were determined after PDT by incubating the cells in white medium DMEM (Biowhittaker LONZA) without serum for 30 min at 37°C containing 5 μM of 5-(and 6)-chloromethyl-2'-7'-dichlorodihydrofluorescein diacetate, acetyl ester CM-H$_2$DCFDA (C6827, Molecular Probes, Invitrogen, Milan, Italy). CM-H$_2$DCFDA was metabolized by non-specific esterases to the non-fluorescence product of 5-(and 6)-chloromethyl-2'-7'-dichlorodihydrofluorescein diacetate, acetyl ester, which was oxidized to the fluorescent product by ROS. Then, the cells were washed twice in PBS, trypsinized, resuspended in PBS and measured for the ROS content by FACS (FACScan, Becton Dickinson, San Josè, USA).

Lipid peroxidation: TBARS and C11-BODIPY$^{581/591}$ assays. The lipid peroxidation assays have been performed according to reported protocols.[11,30,31] Experimental details are reported as Supplementary information (S_5).

Confocal microscopy and MitoTracker. HepG2 cells were plated at density of 10^5 on the cover glass, treated with Fluo-PEG-Pb*a* 5 μM for 24 h, then illuminated for 15 min. After light activation the cells were treated with 100 nM of MitoTracker Red for 30 min at 37°C (Molecular Probes, Invitrogen, Milan, Italy) and then the glasses were prepared. The cells were washed twice with PBS, fixed with 3% paraformaldehyde (PFA) in PBS for 20 min. After washings with 0.1 M glycine, containing 0.02% sodium azide in PBS to remove PFA, and Triton X-100 (0.1% in PBS), the cells were incubated with Hoechst to stain the nuclei. The cells were analysed using a Leica TCS SP1 confocal imaging system, Exc laser Argon 488 nm (to see fluorescein) and laser He-Ne 543 nm (to see MitoTracker).

Mitochondria membrane depolarization. mPEG-Pb*a* or Pb*a*/PDT treated cells (plated at 2 x 10^5 cells) were loaded with 10 μg/ml JC-1 (Molecular Probes, Leiden) for 30 min at 37°C in PBS buffer. The cells were washed twice with fresh PBS. Flow cytometry was performed 24 h after light activation using a FACScan (Becton-Dickinson, San Jose, USA) equipped with a single 488 nm argon laser. A minimum of 10,000 cells for sample was acquired in list mode and analyzed using Cell Quest software. The cell population was chosen by FSC light and SSC light. The signal was detected by FL1 and FL2 channel in log scale. The dye JC-1, excited by the argon laser emits in FL-1 (monomer, typical low $\Delta\psi$) and FL-2 (aggregates, whose formation is due to a high $\Delta\psi$).

In vitro stability studies. To investigate the hydrolytic stability of mPEG-Pb*a*, 5 mg/ml was dissolved in phosphate buffer, pH 7.4 (0.005 M Na_2HPO_4 - 0.001 M KH_2PO_4, adjusted to pH 7.4 with NaOH) at 37 ± 0.1°C.[38] Samples were taken at suitable intervals and the quantity of Pb*a* released by hydrolysis was quantified with HPLC method with some modification.[35] Briefly: Separation was performed at room temperature by using AcCN- acetone (45:55 v/v) as the mobile phase at a flow rate 0.6 ml/min and detection wavelength was 409 nm. A LiChrosorb RP18 (Perkin-Elmer) 250 x 4.6 mm ID column packed with 10 μm particle size was used. The amounts of the Pb*a* released was analyzed and calculated by comparing the slope of the standard curve.

In vivo studies. Female C57/BL6, 6–8 weeks old, were obtained from Charles River, Calco, Italy. All the experimental procedures were done in compliance with the guidelines of European (86/609/EEC) and Italian (D.L.116/92) laws and were approved by the Italian Ministry of University and Research as well as by the Administration of the University Animal Facility.

Tissue distribution. Pb*a* and mPEG-Pb*a* conjugate (50 μmol/kg in terms of Pb*a* molecule) were solubilized in saline solution-DMSO (9 + 1 v/v) respectively, also other mPEG-Pb*a* conjugate (equivalent 50 μmol/kg of Pb*a*) in saline solution, and administered by i.p. (intraperitoneal injection) at the mice. The animals were sacrificed by cervical dislocation at different time points (1, 3, 6 and 24 h) (six mice at 0 h, no injection and three mice at the other time points), after administration. The brain, spleen, kidney, duodenum, lung and the liver were removed, washed in PBS and stored at -80°C. About 200 mg of tissues were homogenized in MeOH-DMSO (4 + 1 v/v). The homogenates were centrifuged at 3,000 g/rev at 4°C for 15 min., and the fluorescence of the supernatant was measured setting the excitation wavelength at 409 nm and recording the emission spectrum from 400 and 750 nm. In all the case Pb*a* amounts were determined by interpolation of emission intensity and Pb*a* concentration plotted on a standard curve.

Spectrofluorimetric determination of mPEG-Pb*a* and Pb*a* in tissues. A Jasko luminescence spectrofluorimeter was used for the measurement of the fluorescence intensity of biological samples.[34] The supernatant of the tissue extract was transferred into a 3 ml quartz cuvette (1 cm pathlenght) and the fluorescence intensity was measured using excitation and emission wavelengths of 409 and 670 nm respectively. Methanol-DMSO (4 + 1 v/v) was used as the blank. A stock standard solution of mPEG-Pb*a* was made by dissolving the adduct (12.5 mg; 1.25 mg of Pb*a*) in distillate water (100 ml). Aliquots of the stock standard solution

were diluted with methanol-DMSO (4 + 1 v/v) to give working standard solutions with a range of concentrations between 0.50 and 25.0 μg/ml. These were used to construct a calibration curve for the determination on mPEG-Pb*a*. In analogue manner was constructed a calibration curve for the determination of Pb*a* solution of start 12.5 mg in methanol-DMSO (4 + 1 v/v) (100 ml). Pb*a* and mPEG-Pb*a* amounts, in different tissues, were determined by interpolation of emission intensity and Pb*a* concentration plotted on a standard curve.

Mice preparation for optical imaging scan. Female mice C57/BL6 6–8 weeks old, were anesthetized using a gaseous anaesthesia system (Biological Instruments, Italy), based on isoflurane mixed to oxygen and nitrogen protoxide. Anaesthesia was first inducted in a pre-anaesthesia chamber and after the mouse was placed inside the eXplore Optix with isoflurane percentage respectively of 2% and 1%. Later, mice were shaved in the regions of interest because hair cause laser scattering. A first blank image has been acquired before treating the animals, then the experimental mice were injected intraperitoneally with 50 μmol/Kg of Pb*a* and mPEG-Pb*a*.

In vivo time-domain optical imaging. The small-animal time-domain eXplore Optix pre-clinical imager was used in this study. In all imaging experiments a 670 nm pulsed laser diode with a repetition frequency of 80 MHz and a time resolution of 12 ps light pulse was used for excitation. The fluorescence emission at 700 nm was collected and detected through a fast photomultiplier tube and a highly sensitive time-correlated single-photon counting system. Two-dimensional scanning regions of interest (ROI) were selected, laser power, integration time and scan step were optimized according to the signal emitted. The data were recorded as temporal point-spread functions, and the images were reconstructed as fluorescence intensity and fluorescence lifetime. Prior to inject the probe or the labelled cells, mice were imaged to obtain a background scan. Mice were imaged daily overtime to visualize the biodistribution and the sites of accumulation. The background signal intensity recorded with the baseline image for each animal before the injection of the probe was subtracted from each post-contrast image, EXplore Optix™* *OptiView* software (GE Healthcare) was used[39] to estimate fluorescence intensity and lifetime. The fluorescence lifetime analysis was based on a single or two exponential fitting models applied to the temporal point-spread function.[40]

The intensity maps of acquired data were compared as normalized counts (NC) working on multiple images. Namely, for NC the photon counts over the Temporal Point spread Function (TPSF) curves were normalized with laser power and integration time, while scan step remained constant.

Acknowledgements

This work has been carried out with the financial support of PRIN 2007, FVG L11/2005.

Note

Supplementary materials can befound at:
www.landesbioscience.com/supplement/RapozziCBT10-5-sup.pdf

Supporting Information Description

Figures S_1: proliferation data of cells treated with mPEG-Pb*a*; S_2: caspase-3/7 activation and time lapse microscopy; S_3: imaging; S_4: 1H-NMR, fluoscence spectra of Fluo-PEG-Pba; S_5, protocol for lipid peroxidation assay.

References

1. Tandon YK, Yang MF, Baron ED. Role of photodynamic therapy in psoriasis: a brief review. Photodermatol Photoimmunol Photomed 2008; 24:222-30.
2. Cruess AF, Zlateva G, Pleil AM, Wirostko B. Photodynamic therapy with verteporfin in age-related macular degeneration: a systematic review of efficacy, safety, treatment modifications and pharmacoeconomic properties. Acta Ophthalmol 2009; 87:118-32.
3. O'Connor AE, Gallagher WM, Byrne AT. Porphyrin and nonporphyrin photosensitizers in oncology: preclinical and clinical advances in photodynamic therapy. Photochem Photobiol 2009; 85:1053-74.
4. Dolmans DE, Fukumura D, Jain RK. Photodynamic therapy for cancer. Nat Rev Cancer 2003; 3:380-7.
5. Dougherty TJ, Gomer CJ, Henderson BW, Jori G, Kessel D. Korbelik M, et al. Photodynamic therapy. J Natl Cancer Inst 1998; 90:889-905.
6. Jori G. Photodynamic therapy of microbial infections: state of the art and perspectives. J Environ Pathol Toxicol Oncol 2006; 25:505-19.
7. Josefsen LB, Boyle RW. Photodynamic therapy and the development of metal-based photosensitisers. Met Based Drugs 2008; 2008:276109-33.
8. Castano AP, Demidova TN, Hamblin MR. Mechanisms in photodynamic therapy: part one-photosensitizers, photochemistry and cellular localization. Photodiagn Photodyn Ther 2004; 1:279-93.
9. Castano AP, Demidova TN, Hamblin MR. Mechanisms in photodynamic therapy: part three-photosensitizers pharmacokinetics, biodistribution, tumor localization and modes of tumor destruction. Photodiagn Photodyn Ther 2005; 2:91-106.
10. Detty MR, Gibson SL, Wagner SJ. Current clinical and preclinical photosensitizers for use in photodynamic therapy. J Med Chem 2004; 47:3897-915.
11. Rapozzi V, Miculan M, Xodo LE. Evidence that photoactivated pheophorbide a causes in human cancer cells a photodynamic effect involving lipid peroxidation. Cancer Biol Ther 2009; 14:1-10.
12. Tang PM, Chan JY, Au SW, Kong SK, Tsui SK, Waye MM, et al. Pheophorbide *a*, an active compound isolated from *Scutellaria barbata*, possesses photodynamic activities by inducing apoptosis in human hepatocellular carcinoma. Cancer Biol Ther 2006; 5:1111-6.
13. Radestock A, Elsner P, Gitter B, Hipler UC. Induction of apoptosis in HaCaT cells by photodynamic therapy with chlorin e6 or pheophorbide a. Skin Pharmacol Physiol 2007; 20:3-9.
14. Tang PM, Liu XZ, Zhang DM, Fong WP, Fung KP. Pheophorbide a based photodynamic therapy induces apoptosis via mitochondrial-mediated pathway in human uterine carcinosarcoma. Cancer Biol Ther 2009; 8:533-9.
15. Li WT, Tsao HW, Chen YY, Cheng SW, Hsu YCA. Study on the photodynamic properties of chlorophyll derivatives using human hepatocellular carcinoma cells. Photochem Photobiol Sci 2007; 6:1341-8.
16. Hajri A, Coffy S, Vallat F, Evrard S, Marescaux J, Aprahamian M. Human pancreatic carcinoma cells are sensitive to photodynamic therapy in vitro and in vivo. Br J Surg 1999; 86:899-906.
17. Tang PMK, Zhang DM, Xuan NB, Tsui SKW, Waye MMY, Kong SK, et al. Photodynamic therapy inhibits p-glycoprotein mediated multidrug resistance via JNK activation in human hepatocelluklar carcinoma using the photosensitizer pheophorbide a. Mol Cancer 2009; 8:56-67.
18. Hajri A, Wack S, Meyer C, Smith MK, Leberquier C, Kedinger M, et al. In vitro and in vivo efficacy of Photofrin and Pheophorbide a, a bacteriochlorin, in photodynamic therapy of colonic cancer cells. Photochem Photobiol 2002; 75:140-8.
19. Evrard S, Keller P, Hajri A, Balboni G, Mendoza-Burgos L, Damge C, et al. Experimental pancreatic cancer in the rat treated by photodynamic therapy. Br J Surg 1994; 81:1185-9.
20. Veronese FM, Mero A. The impact of PEGylation on biological therapies. Biodrugs 2008; 22:315-29.
21. Greenwald RB, Conover CD, Pendri A, Choe YH, Martinez A, Wu D, et al. Drug delivery of anticancer agents: water soluble 4-poly(ethylene glycol) derivatives of the lignin, podophyllotoxin. J Control Release 1999; 61:281-94.
22. Chinol M, Casalini P, Maggiolo M, Canevari S, Omodeo ES, Caliceti P, et al. Biochemical modifications of avidin improve pharmacokinetics and biodistribution and reduce immunogeni city. Br J Cancer 1998; 78:189-97.
23. Delgado C, Francis GE, Fisher D. The uses and properties of PEG-linked proteins. Crit Rev Ther Drug Carrier Syst 1992; 9:249-304.

24. Tsutsumi Y, Kihira T, Tsunoda S, Kamada H, Nakagawa S, Kaneda Y, et al. Molecular design of hybrid tumor necrosis factor-alpha III: polyethylene glycol-modified tumor necrosis factor-alpha has markedly enhanced antitumor potency due to longer plama half-life and higher tumor accumulation. J Pharmacol Exp Ther 1996; 278:1006-11.
25. Hamblin MR, Miller JL, Rizvi I, Loew HG, Hasan T. Pegylation of charged polymer-photosensitiser conjugates:effects on photodynamuic efficacy. Br J Cancer 2003; 89:937-43.
26. Bonora GM, Campaner P, Drioli S. Bifunctional derivatives of polyethylene glycol, their preparation and use 2005; WO 2005/123139 A1.
27. Röder B, Hanke T, Oelckers S, Hackbarth S, Symietz C. Photophysical properties of pheophorbide a in solution and in model membrane systems. J Porphyrins Phthalocyanines 2000; 4:37-44.
28. Soukos NS, Hamblin MR, Hasan T. The effect of charge on cellular uptake and phtotxicity of polylysine chlorine e6 conjugates. Photochem Photobiol 1997; 65:723-2934.
29. Wong SHY, Knight JA, Hopfer SM, Zaharia O, Leach CN, Sunderman FW. Lipoperoxides in plasma as measured by liquid-chromatographic separation of malondialdehyde-thiobarbituric acid adduct. Clin Chem 1987; 33:214-20.
30. Drummen GPC, Liebergen LCM, Op den Kamp JAF Post JA. C11-Bodipy$^{581/591}$, an oxidation-sensitive fluorescence lipid peroxidation probe: (micro)spectroscopic characterization and validation of methodology. Free Rad Biol Med 2002; 33:473-90.
31. Pap EHW, Drummen GPC, Winter VJ, Kooij TWA, Rijken P, Wirtz KWA, et al. Ratiofluorescence microscopy of lipid oxidation in living cells using C11-BODIPY$^{581/591}$. FEBS Lett 1999; 453:278-82.
32. Naguib YMA. A fluorimetric method for measurement of peroxyl radical scavenging activities of lipophilic antioxidants. Anal Biochem 1998; 265:290-8.
33. Lugli E, Troiano L, Ferraresi R, Roat E, Prada N, Nasi M, et al. Characterization of cells with different mitochondrial membrane potential during apoptosis. Cytometry 2005; 68:29-35.
34. Cai H, Lim CK. Comparison of HPLC, capillary electrophoretic and direct spectrofluorimetric methods for the determination of temoporfin- poly(ethylene glycol) conjugates in plasma. The Analyst 1998; 123:2243-5.
35. Yoshitake Y, Kakiuchi K, Morishige K, Gohda S, Shigematsu T, Nishikawa Y. Determination of pheophorbide a and methylpheophorbide a by fluorescence high performance liquid chromatography: availability of narrow baseline method. Analytical Sciences 1986; 2:67-9.
36. Aprahamian M, Evrard S, Keller P, Tsuji M, Balboni G, Damge C, Marescaux J. Distribution of pheophorbide A in normal tissues and in experimental pancreatic cancer in rats. Anticancer Drug Des 1993; 8:101-14.
37. Bonora GM, Campaner P, Drioli S. Synthesis of Selectively End-Modified High-Molecular Weight Polyethyleneglycole. Lett Org Chem 2006; 3:773-9.
38. Zacchigna M, Cateni F, Di Luca G, Voinovich D, Perissutti B, Drioli S, et al. Synthesis of a new mPEG-Dexamethasone Conjugate and preliminary bioavailability studies in rabbits. J Drug Delivery Science and Techn 2008; 18:155-9.
39. Lam S, Lesage F, Intes X. Time-domain fluorescent diffuse optical tomography: analytical expressions. Optics Express 2005; 13:2263-75.
40. Abulrob A, Brunette E, Slinn J, Baumann E, Stanimirivic D. In vivo time domain optical imaging of renal ischemia-reperfusion injury: discrimination based on fluorescence lifetime. Mol Imaging 2007; 6:304-14.